

Crystal Growth & Design Manuscript Draft

Title: Coupling Viedma Ripening with Racemic Crystal Transformations: Mechanism of Deracemization

Authors: Christos Xiouras[†], Joop H. Ter Horst[‡], Tom Van Gerven[†] and Georgios D. Stefanidis^{†*}

[†] Process Engineering for Sustainable Systems (ProcESS), Department of Chemical Engineering KU Leuven, Celestijnenlaan 200F, 3001 Leuven, Belgium

[‡] EPSRC Centre for Innovative Manufacturing in Continuous Manufacturing and Crystallisation (CMAC), Strathclyde Institute of Pharmacy and Biomedical Sciences (SIPBS), Technology and Innovation Centre, University of Strathclyde, 99 George Street, Glasgow G1 1RD, U.K.

*Correspondence to: Georgios D. Stefanidis

Tel: +32(0)16321007

E-mail: Georgios.Stefanidis@cit.kuleuven.be

Type of Manuscript: Article

Keywords: Crystal transformation, Viedma ripening, deracemization, racemic compounds

Abstract: It has been recently observed that coupling Viedma ripening with a seeded in-situ metastable racemic crystal to conglomerate transformation leads to accelerated and complete deracemization: crystal transformation-enhanced deracemization. By means of a simple kinetic model, we show that the mechanistic pathway of this new process depends profoundly on the interplay between the crystal transformation and racemization processes, which in turn influence the nucleation process of the counter enantiomer. If the nucleation of the counter enantiomer is suppressed (e.g. by sufficiently fast racemization, low amount of racemic compound or gradual feed, low relative solubility between racemic compound and conglomerate), deracemization proceeds via a second order asymmetric transformation (SOAT) and is limited primarily by the dissolution rate of the racemic crystals and the growth rate of the preferred enantiomer crystals. Breakage and agglomeration accelerate the process, but contrary to conventional Viedma ripening, they are not essential ingredients to explain the observed enantiomeric enrichment. If the nucleation process of the counter enantiomer is not sufficiently suppressed, deracemization is initially controlled by the dissolution rate of the racemic crystals, but Viedma ripening is subsequently required to convert the conglomerate crystals of the counter enantiomer formed by nucleation, resulting in slower deracemization kinetics. In both cases, the combined process leads to faster deracemization kinetics compared to conventional Viedma ripening, while it autocorrects for the main disadvantage of SOAT, i.e. the accidental nucleation of the counter enantiomer. In addition, crystal transformation-enhanced deracemization extends the range of applicability of solid-state deracemization processes to compounds that form metastable racemic crystals.

Coupling Viedma Ripening with Racemic Crystal Transformations: Mechanism of Deracemization

Christos Xiouras[†], Joop H. Ter Horst[‡], Tom Van Gerven[†] and Georgios D. Stefanidis^{†,*}

[†] Process Engineering for Sustainable Systems (ProcESS), Department of Chemical Engineering KU Leuven, Celestijnenlaan 200F, 3001 Leuven, Belgium

[‡] EPSRC Centre for Innovative Manufacturing in Continuous Manufacturing and Crystallisation (CMAC), Strathclyde Institute of Pharmacy and Biomedical Sciences (SIPBS), Technology and Innovation Centre, University of Strathclyde, 99 George Street, Glasgow G1 1RD, U.K.

*Correspondence to: Georgios D. Stefanidis

Tel: +32(0)16321007, Email: Georgios.Stefanidis@cit.kuleuven.be

KEYWORDS: Crystal transformation, Viedma ripening, deracemization, racemic compounds

ABSTRACT

It has been recently observed that coupling Viedma ripening with a seeded in-situ metastable racemic crystal to conglomerate transformation leads to accelerated and complete deracemization: *crystal transformation-enhanced deracemization*. By means of a simple kinetic model, we show that the mechanistic pathway of this new process depends profoundly on the interplay between the crystal transformation and racemization processes, which in turn influence the nucleation process of the counter enantiomer. If the nucleation of the counter enantiomer is

suppressed (*e.g.* by sufficiently fast racemization, low amount of racemic compound or gradual feed, low relative solubility between racemic compound and conglomerate), deracemization proceeds via a second order asymmetric transformation (SOAT) and is limited primarily by the dissolution rate of the racemic crystals and the growth rate of the preferred enantiomer crystals. Breakage and agglomeration accelerate the process, but contrary to conventional Viedma ripening, they are not essential ingredients to explain the observed enantiomeric enrichment. If the nucleation process of the counter enantiomer is not sufficiently suppressed, deracemization is initially controlled by the dissolution rate of the racemic crystals, but Viedma ripening is subsequently required to convert the conglomerate crystals of the counter enantiomer formed by nucleation, resulting in slower deracemization kinetics. In both cases, the combined process leads to faster deracemization kinetics compared to conventional Viedma ripening, while it autocorrects for the main disadvantage of SOAT, *i.e.* the accidental nucleation of the counter enantiomer. In addition, crystal transformation-enhanced deracemization extends the range of applicability of solid-state deracemization processes to compounds that form metastable racemic crystals.

1. INTRODUCTION

Attrition-enhanced deracemization (Viedma ripening) is an isothermal re-crystallization process that allows the complete conversion of a racemic suspension of conglomerate crystals to an enantiopure solid phase by contact with an attrition source, *e.g.* stirring in the presence of grinding media ¹. Compared to other crystallization methods applied for chiral resolution, it offers significant advantages, *i.e.* superior yield, no need for heating/cooling or extensive knowledge of solid-liquid equilibria ^{2,3}. Viedma ripening was first demonstrated for sodium

chlorate, an intrinsically achiral compound that crystallizes as conglomerate crystals, but has since then been modified to work also for intrinsically chiral compounds *e.g.* amino acids ⁴⁻⁷ and pharmaceuticals ⁸⁻¹⁰ that crystallize as conglomerate crystals by incorporating a fast racemization reaction. The outcome of the deracemization process depends on the initial conditions ^{11,12}: mass or crystal size distribution (CSD) imbalance between the enantiomers ^{1,13-15}, presence of chiral impurities ¹⁶ or additives ¹⁷⁻¹⁹ or circularly polarized light ²⁰. In addition, the total time to enantiopurity varies drastically for different compounds, sometimes leading to very long processing times. A different approach for complete deracemization is preferential crystallization with in-situ racemization, termed as second order asymmetric transformation (SOAT) ²¹⁻²³. In this process, seeding of the preferred enantiomer in a supersaturated racemic solution allows for selective nucleation/growth of only that enantiomer ²⁴. The main disadvantage of this process is that primary nucleation of the counter enantiomer can occur ²⁵. The application of in-situ grinding in SOAT processes has been shown to suppress the nucleation of the counter enantiomer up to a certain extent ^{26,27}, while it can also function as a “safety catch” for SOAT leading to complete deracemization through Viedma ripening ²⁸.

Vital prerequisites for both Viedma ripening of chiral compounds and SOAT are solution phase racemization and conglomerate crystallization ²⁹. However, most chiral compounds, when crystallized from a racemic solution, form racemic compounds ²² (i.e. individual crystals contain both enantiomers in equal amounts), although for some compounds both crystal forms can appear depending on the crystallization conditions. Recently, it was shown that the combination of a solvent-mediated metastable racemic crystal transformation to conglomerate coupled with Viedma ripening can still lead to full deracemization, despite the presence of the racemic compound: *crystal transformation-enhanced deracemization* ^{30,31}. Remarkably, the rate of

deracemization is also considerably faster when the transformation is included. Solvent-mediated crystal transformations proceed via the simultaneous dissolution of the metastable phase and the nucleation/growth of the stable phase³², in this case the dissolution of the metastable racemic compound and the growth and nucleation of the stable racemic conglomerate. The relative rates between these processes ultimately define the kinetics of the transformation^{33,34}. Since an essential prerequisite for the nucleation and growth is the existence of supersaturation, the process has distinct characteristics from Viedma ripening, the latter being a near-equilibrium process taking place at low supersaturation where nucleation is no longer possible^{2,35}. It is currently unclear whether the mechanisms thought to be crucial in Viedma ripening (breakage, agglomeration) are also essential for the crystal transformation-enhanced deracemization process and so is the influence of the crystal transformation kinetics on the deracemization process. Additionally, the crystal transformation-enhanced deracemization process offers significant advantages compared to conventional Viedma ripening as it extends the applicability of solid-state deracemization processes to compounds that form racemic crystals and undergo similar transformations. Furthermore, once the process is optimized, it could lower the total deracemization time, which in turn may allow for less intense grinding and a more practical and scalable (continuous) deracemization process.

The autocatalytic enantiomeric excess amplification occurring in the conventional Viedma ripening process has been modelled using kinetic rate equations³⁶⁻⁴⁰, agent-based models⁴¹, Monte Carlo simulations^{35,42-44}, dispersive kinetic models⁴⁵ and population balance models⁴⁶⁻⁴⁹. Almost all models take into account racemization, size-dependent solubility, attrition and enantioselective agglomeration to explain the experimentally observed results. Most reports conclude that the latter mechanism is essential to explain the exponential enantiomeric excess

increase. One of the simplest models for Viedma ripening, first postulated by Uwaha ³⁶, and extended for chiral compounds by Noorduyn and McBride ³⁹ is the cluster model, which assumes the existence of small subcritical clusters that retain chirality and incorporate to larger crystals of the same chirality. Despite its simplicity, the (modified) cluster model has, over the years, been used to explain several intriguing experimental findings in deracemization studies such as deracemization due to temperature cycling ⁵⁰, persistent reverse enantiomeric excess in solution ⁵¹, linear deracemization kinetics in the presence of chiral additives ¹⁸ and chiral resolution in a coupled batch grinding process ⁵².

The aim of this study is to elucidate the general mechanisms through which deracemization occurs when a seeded solvent-mediated racemic crystal transformation to conglomerate takes place under grinding/racemization conditions. In particular, we focus on the effect of the crystal transformation and on the influence of the various mechanisms thought to be active in Viedma ripening, namely: breakage, agglomeration and racemization. To this end, we develop a kinetic model, based on the cluster model, to account for both Viedma ripening and the crystal transformation-enhanced deracemization. We show that the model can qualitatively reproduce the recent experimental observations. The new process is then compared with Viedma ripening, leading to important mechanistic insights. Finally, we underline the crucial role of nucleation on the deracemization mechanism and kinetics of new process and we show that a careful control of the crystal transformation process can lead to fast deracemization rate. The results presented here offer more understanding into the mechanism and optimization of the new crystal transformation-enhanced deracemization process.

2. MODEL DESCRIPTION

In order to simulate and compare the evolution of the enantiomeric excess ε using conventional Viedma ripening and the crystal transformation-enhanced deracemization process, we adapt the simple cluster model postulated by Uwaha, McBride and Noorduin^{36,39}. The model is extended to include a solvent-mediated racemic crystal transformation to conglomerate.

We consider a partially resolved solid mixture consisting of a population of racemic compound crystals together with crystals of a single enantiomer, which is brought in contact with a solvent at a constant temperature T and pressure p . We assume that in the given suspension at temperature T , the racemic compound and the racemic conglomerate are monotropically related (or enantiotropically related with T being far from the transition temperature) and that the racemic compound is metastable with respect to the conglomerate. The batch system is perfectly mixed and grinding of the crystals maintains a very small crystal size.

The actual crystal size distributions (CSD) for each enantiomer of the conglomerate crystals are simplified by considering only two arbitrary groups of sizes: large crystals and small chiral clusters³⁹. The large crystals in the initially present CSD correspond to the conglomerate seeds, typically of a single chirality, since they are used to control the deracemization outcome. The small chiral clusters correspond to the fragments formed by ablation of large conglomerate crystals or by nucleation due to the supersaturation generated by the dissolution of the metastable racemic crystals.

In the deracemization process model, the mass of each chiral species per suspension volume (mg mL^{-1}) in the metastable racemic crystals, large conglomerate crystals, small chiral clusters and the solution phases, as functions of time (h), are denoted as $C_i^R(t)$, $C_i^B(t)$, $C_i^S(t)$ and $C_i^{liq}(t)$, respectively with $i=1,2$ indicating enantiomers D and L , respectively. Since the racemic crystals

by definition contain equal amounts of molecules of both chiralities, it follows that at any given time: $C_1^R(t) = C_2^R(t)$. The system is described by the following set of coupled differential equations considering: growth/dissolution of the metastable racemic crystals with rate G_i^R , nucleation of clusters with rate J_i , growth/dissolution of clusters and crystals with rates G_i^S and G_i^B , respectively, breakage of large crystals with rate B_i , agglomeration of clusters with each other and with crystals of the same chirality with rate A_i , and solution phase racemization with rate r_i .

$$\frac{dC_i^R(t)}{dt} = G_i^R(t) \quad (1)$$

$$\frac{dC_i^B(t)}{dt} = G_i^B(t) - B_i(t) + A_i(t) \quad (2)$$

$$\frac{dC_i^S(t)}{dt} = J_i(t) + G_i^S(t) + B_i(t) - A_i(t) \quad (3)$$

$$\frac{dC_i^{liq}(t)}{dt} = -G_i^R(t) - G_i^B(t) - G_i^S(t) - J_i(t) - r_i(t) \quad (4)$$

$$\sum_{i=1}^2 [C_i^R(t) + C_i^B(t) + C_i^S(t) + C_i^{liq}(t)] = const. \quad (5)$$

Equation 5 describes the mass conservation in the system. A schematic representation of all the underlying rate processes and mass transfer considered in the deracemization process model for Viedma ripening and the coupled transformation/Viedma ripening process is provided in Figure 1. We note that since all variables in the model equations 1-5 are total masses in the system, the size and number change of crystals/clusters cannot be explicitly described using this model. In

addition, concentration and time units were arbitrarily chosen to be mg mL^{-1} and h, respectively, but the choice of any other units for concentration and time would not change the qualitative character of the model. The units of the rates ($\text{mg mL}^{-1} \text{ h}^{-1}$) and rate constants described henceforth depend on the concentration and time units chosen.

The deracemization process model presented here has the ingredients to describe both conventional Viedma ripening, and Viedma ripening coupled with a solvent-mediated racemic crystal transformation to racemic conglomerate (new process). Simply by setting $G_i^R(t)$, $J_i(t)$ and $C_i^R(t)$ to zero and starting with the desired initial mass of conglomerate crystals, the model reduces to the simple cluster model that has been previously postulated by Uwaha, McBride and Noorduyn to describe Viedma ripening^{36,39}. As Viedma ripening is a near-equilibrium process, nucleation can be considered negligible for the case in which no crystal transformation takes place ($J_i(t) = 0$)³⁵.

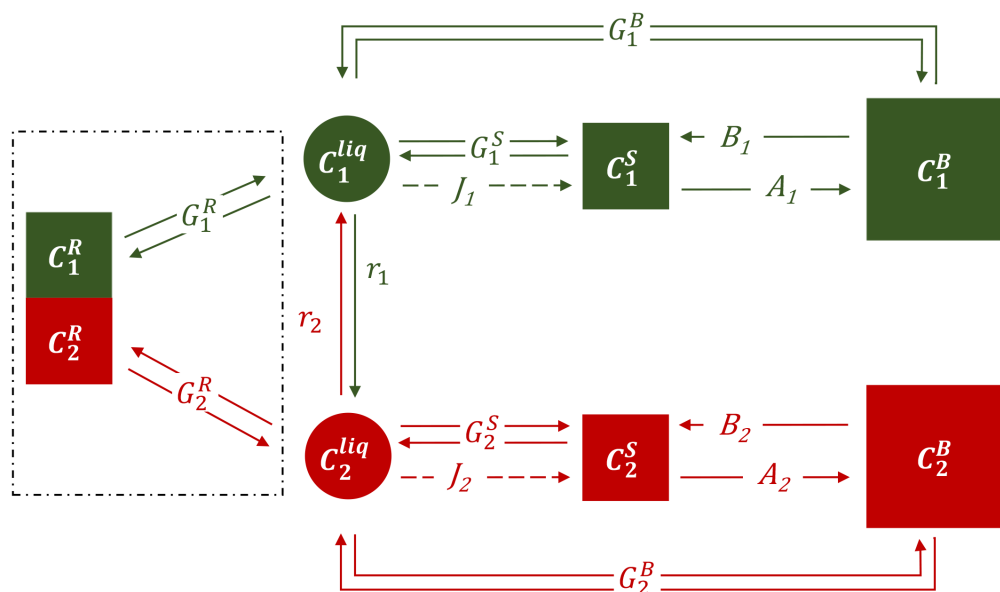


Figure 1. Rate processes and mass transfer involved in a Viedma ripening process ($i=1,2$ for D and L enantiomers, respectively). For the (optional) combination of Viedma ripening with a metastable racemic crystal transformation the additional processes in the dashed box also occur, together with nucleation at a rate J_i (dashed arrows).

Growth and dissolution

The growth and dissolution rates ($\text{mg mL}^{-1} \text{h}^{-1}$) of large conglomerate crystals and small clusters G_i^B and G_i^S , respectively are considered linear and proportional to the difference in concentrations of D or L enantiomers in solution and the equilibrium concentration (solubility) in a solution with crystals or clusters, C_{eq}^B and C_{eq}^S , respectively:

$$G_i^B(t) = \alpha(C_i^{liq}(t) - C_{eq}^B)C_i^B(t) \quad (6)$$

$$G_i^S(t) = \alpha(C_i^{liq}(t) - C_{eq}^S)C_i^S(t) \quad (7)$$

Where α is the growth/dissolution rate constant ($\text{mL mg}^{-1} \text{h}^{-1}$) for the conglomerate. In Equations 6-7, when the driving force is positive: $(C_i^{liq} - C_{eq}^{B,S}) > 0$, growth occurs, while the case of $(C_i^{liq} - C_{eq}^{B,S}) < 0$, corresponds to the dissolution of mass. It is noted that since enantiomers have identical thermodynamic properties, C_{eq}^B and C_{eq}^S have the same values for both D and L . Similarly to previous models^{18,39,51,52}, due to the Gibbs-Thomson effect, the cluster solubility $C_{eq}^S > C_{eq}^B$ is considered to be slightly higher than that of the large crystals, leading to slightly faster dissolution kinetics for the clusters in comparison with an equal mass of large crystals. In all simulations, C_{eq}^S was assumed to be 10% higher than C_{eq}^B ($C_{eq}^B = 2 \text{ mg mL}^{-1}$, while $C_{eq}^S = 2.2 \text{ mg mL}^{-1}$), following the study of Hein et al. who observed $\approx 10\%$ solubility increase when grinding a

slurry of large crystals of a chiral organic compound¹⁴. Following Meyerhoffer's double solubility rule⁵³, the solubility of the racemic conglomerate is assumed to be twice that of the pure enantiomers.

The growth/dissolution rate ($\text{mg mL}^{-1} \text{h}^{-1}$) of the racemic crystals is considered proportional to the difference in the concentration between the racemic part of the solution phase and the (metastable) equilibrium concentration in a solution with racemic crystals, C_{eq}^R :

$$G_i^R(t) = \alpha' \left((1 - \varepsilon_l(t)) \sum_{i=1}^2 C_i^{liq}(t) - C_{eq}^R \right) C_i^R(t) \quad (8)$$

Where α' is the growth/dissolution rate constant ($\text{mL mg}^{-1} \text{h}^{-1}$) for the racemic crystals, C_{eq}^R is the (metastable) equilibrium concentration of *D* and *L* enantiomers together in the solution phase in contact with racemic crystals and ε_l is the liquid phase enantiomeric excess defined as:

$$\varepsilon_l(t) = \frac{|C_1^{liq}(t) - C_2^{liq}(t)|}{\sum_{i=1}^2 C_i^{liq}(t)} \quad (9)$$

Unless stated otherwise, the (metastable) solubility of the racemic crystals is considered in all simulations to be slightly higher than double that of the pure enantiomer clusters ($C_{eq}^R = 4.7 \text{ mg mL}^{-1}$) so that the clusters are more stable than the racemic compound²².

Breakage and agglomeration

The crystal breakage rate ($\text{mg mL}^{-1} \text{h}^{-1}$) is assumed to be proportional to the concentration C_i^B of large enantiomer crystals:

$$B_i(t) = \beta C_i^B(t) \quad (10)$$

Where β is the breakage rate constant (h^{-1}). For simplicity, no breakage or size effects are assumed to occur for the racemic crystals, which are only consumed by dissolution.

Agglomeration is considered to be second order and to occur only in an enantioselective manner among chiral clusters (self-agglomeration) and between chiral crystals and clusters. The contribution of both terms in the agglomeration rate ($\text{mg mL}^{-1} \text{h}^{-1}$) is described by Equation 11:

$$A_i(t) = \gamma C_i^B(t) C_i^S(t) + \nu' C_i^S(t)^2 \quad (11)$$

Where γ and ν' are the agglomeration rate constants ($\text{mL mg}^{-1} \text{h}^{-1}$).

Nucleation

In modelling the combined crystal transformation - deracemization process, nucleation cannot be neglected, because the dissolution of the racemic compound will eventually result in the buildup of significant supersaturation and eventually in the nucleation of conglomerate crystals of both chiralities. Conglomerate crystals of the counter enantiomer are not present initially, therefore primary nucleation is required for their formation, while for the preferred enantiomer secondary nucleation and crystal growth will be dominant in reducing the supersaturation. In this study, secondary nucleation of the major enantiomer is assumed to be driven mainly by attrition and thus no additional expression for secondary nucleation was used. The primary nucleation rate can be described by a Becker-Döring type of model using the simplified expression, valid for supersaturated solutions of sparingly soluble substances: $J_0 = k_n(C - C^*)^n$, where k_n is the nucleation rate constant, C is the solution concentration, C^* is the solubility and n is the

nucleation order ⁵⁴. A similar expression has been adapted by Uwaha ⁵⁵ to describe nucleation in chiral symmetry breaking crystallization processes assuming $n = 2$. Such expressions have also been used in the literature to describe nucleation of the stable polymorph during modelling of solvent-mediated polymorph transformations ⁵⁶. Here, we assume a similar expression for the nucleation rate ($\text{mg mL}^{-1} \text{h}^{-1}$) of chiral clusters:

$$J_i(t) = \nu(C_i^{liq}(t) - C_{eq}^S)^2 \quad (12)$$

Where ν is the nucleation rate constant ($\text{mL mg}^{-1} \text{h}^{-1}$). In Equation 12, if the concentration of either enantiomer is lower than the solubility ($C_{D,L}^{liq} - C_{eq}^S < 0$), for instance in an undersaturated solution, the nucleation rate is set to zero in the model. It is mentioned that, no nucleation of the metastable racemic crystals is assumed to occur, as the solution is (under)saturated with respect to the racemic compound.

Racemization

Similarly to previous models, we assume a first order solution-phase racemization reaction, with rate ($\text{mg mL}^{-1} \text{h}^{-1}$), r_i , where the racemization rate constant (h^{-1}), ρ , is equal for the forward and backward reaction:

$$r_1(t) = \rho(C_1^{liq}(t) - C_2^{liq}(t)) \quad (13)$$

$$r_2(t) = \rho(C_2^{liq}(t) - C_1^{liq}(t)) \quad (14)$$

The expressions for the rate processes (Equations 6-14) are substituted to the set of coupled differential Equations 1-4, which are solved numerically using the built-in ODE45 solver in

MATLAB[®] for given sets of the seven rate constant parameters (α' , α , β , γ , ν' , ν and ρ) and initial values for the concentrations. The temporal evolution of the solid-phase enantiomeric excess $\varepsilon_s(t)$ can then be described by:

$$\varepsilon_s(t) = \frac{\left| \left(C_1^B(t) + C_1^S(t) \right) - \left(C_2^B(t) + C_2^S(t) \right) \right|}{\sum_{i=1}^2 [C_i^R(t) + C_i^B(t) + C_i^S(t)]} \quad (15)$$

In Equation 15, the variables $C_1^R(t)$ and $C_2^R(t)$ are also part of the numerator but they cancel each other out. It is noted that the rate expressions used here are simplified and it is thus difficult to ascribe a physical meaning to the rate constants, which mostly have a relative meaning.

3. RESULTS AND DISCUSSION

3.1 Viedma ripening with a simultaneous racemic crystal transformation

Engwerda et al. experimentally studied the effect of a transformation of a racemic compound to a conglomerate on the deracemization of a Schiff base of phenylglycine amide³⁰. They compared two series of experiments: a) conventional Viedma ripening starting with 60 mg mL⁻¹ of *D* and 40 mg mL⁻¹ of *L* of Schiff base and b) Viedma ripening coupled with crystal transformation using 80 mg mL⁻¹ *DL* and 20 mg mL⁻¹ *D* of Schiff base. Both deracemization experiments were conducted at the same conditions: 10 mL of acetonitrile using DBU as racemization catalyst while stirring in the presence of glass beads. At their experimental conditions the racemic *DL* Schiff base of phenylglycine amide converts to the conglomerate crystal form. Figure 2 (right) shows their experimental results for the evolution of the *D* enantiomer mass fraction in the solid phase. It was found that both experiments led to enantiopurity in favor of the enantiomer initially

in excess. In addition, deracemization kinetics were approximately 10 times faster when the crystal transformation was included.

Using the extended cluster model described in the previous Section, we performed simulations for the two deracemization experiments as conducted by Engwerda et al.: a) conventional Viedma ripening (no crystal transformation takes place) and b) deracemization using a simultaneous racemic crystal transformation to conglomerate coupled with Viedma ripening in the presence of seeds of a single chirality. For both simulations, the values of the rate constants ($\alpha' = \alpha = 2 \text{ mL mg}^{-1} \text{ h}^{-1}$, $\beta = 1 \text{ h}^{-1}$, $\gamma = 0.2 \text{ mL mg}^{-1} \text{ h}^{-1}$, $\nu' = 0.01 \text{ mL mg}^{-1} \text{ h}^{-1}$, $\rho = 100 \text{ h}^{-1}$) are kept the same and the initial concentrations of the enantiomers in the clusters and in the liquid phase are set to zero ($C_D^S(0) = C_L^S(0) = C_D^{liq}(0) = C_L^{liq}(0) = 0$). For Viedma ripening, as no racemic compound is involved, we set $C_D^R(t) = C_L^R(t) = 0$ and the simulation is started only with large conglomerate crystals ($C_D^B(0) = 60 \text{ mg mL}^{-1}$ and $C_L^B(0) = 40 \text{ mg mL}^{-1}$) giving an initial solid phase enantiomeric excess $\varepsilon_s(0) = 20\%$. Furthermore, as nucleation is assumed not to occur in Viedma ripening, the value of ν is set to zero. For the combined case of Viedma ripening and crystal transformation, the simulation is started with: 80 mg mL^{-1} of racemic compound ($C_D^R(0) = C_L^R(0) = 40 \text{ mg mL}^{-1}$) and $C_D^B(0) = 20 \text{ mg mL}^{-1}$ giving again $\varepsilon_s(0) = 20\%$, while $C_L^B(0) = 0$ and $\nu = 0.01$.

Figure 2 (left) presents the model results for the two cases, in terms of the evolution of the enantiomeric purity, *i.e.* the fraction of the preferred enantiomer (in this case *D*) in the solid phase. For Viedma ripening (red curve), the enantiomeric purity reaches 100% with sigmoidal kinetics, similarly to previous modelling and experimental works^{5,45}. When Viedma ripening is coupled with crystal transformation (black curve), enantiomeric purity also reaches 100%.

Additionally, deracemization proceeds much faster (by a factor of 10 approximately), when Viedma ripening is coupled with the crystal transformation. Figure 2 also presents a comparison of our model results with the experimental results of Engwerda et al. (Figure 2, right). Similarly to the experimental findings, the model results show significantly faster increase in enantiomeric purity for the case of the combined crystal transformation and Viedma ripening, while the obtained modeling curves bear a strong qualitative similarity to the experimental ones with regard to the kinetics of deracemization. This convinced us that, despite its simplicity, the extended model qualitatively describes the process.

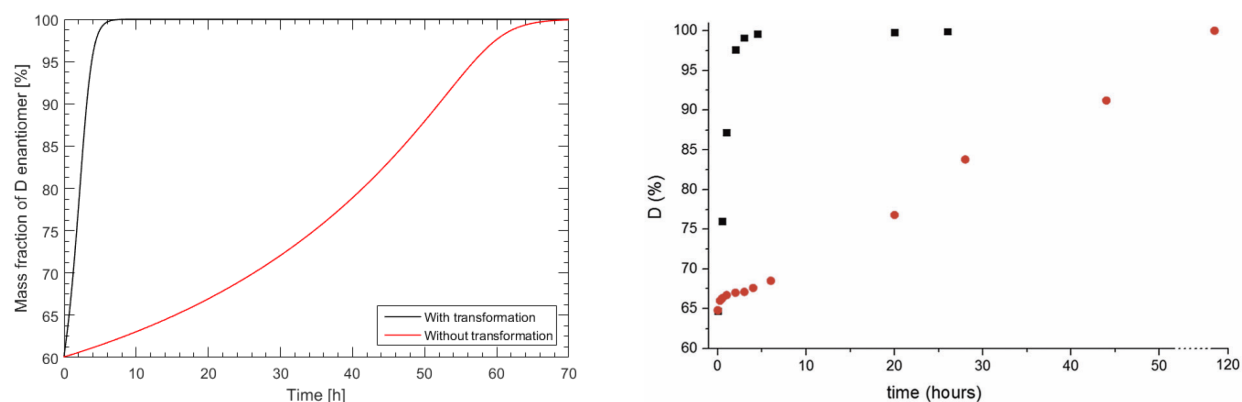


Figure 2. Left: Simulated evolution of the preferred enantiomer (D) solid phase fraction including crystal transformation (black curve) and conventional Viedma ripening without transformation (red curve) at the same conditions. For Viedma ripening (red curve) $v=0$ and $C_D^R(t)=C_L^R(t)=0$. Right: Experimental evolution of the preferred enantiomer (D) solid phase fraction with transformation (black squares) and conventional Viedma ripening without transformation (red squares), reproduced by permission from Engwerda *et al.*, Chem. Commun., **52**, 12049 (2016). Copyright 2016 Royal Society of Chemistry.

In order to obtain more insight into the differences between the two processes, the total solid phase composition and the supersaturation ratio profile for the two enantiomers (defined here as: $S_i(t) = C_i^{liq}(t)/C_{eq}^B$) using the same model parameters as previously are plotted in Figure 3 for both processes.

In the case of Viedma ripening without crystal transformation (Figure 3, top right), the system initially contains conglomerate crystals of both chiralities (60% *D* and 40% *L*) and an initial enantiomeric excess ($\varepsilon_s(0)=20\%$) in favor of the *D* enantiomer. Mass from both crystal populations is initially depleted due to partial dissolution and breakage, while the latter process also gives rise to a mass concentration in clusters of both enantiomers. For the *D* enantiomer, the rate of cluster agglomeration is higher than the *L* enantiomer $A_1 > A_2$. Consequently, the *L* enantiomer has a slightly higher fraction of its mass distributed in clusters and therefore experiences a faster net dissolution rate (clusters are assumed to have a 10% higher solubility than the crystals) giving rise to a slightly higher concentration of the *L* enantiomer in the liquid phase that pertains throughout the deracemization process (Figure 3, bottom right). The excess *L* mass in the liquid phase is continuously converted to their antipode by the fast racemization reaction providing *D* mass for the growth of the *D* enantiomer crystals, which leads to further breakage and agglomeration of the *D* enantiomer sustaining the $A_1 > A_2$ condition. Ultimately, all the molecules in the solid phase convert to a single chirality in an autocatalytic fashion. As pointed out also in previous studies, breakage and agglomeration are required to obtain an increase in ε_s (parameters γ or ν' and β must be non-zero in the model). Additionally, in the conventional Viedma ripening, a slight supersaturation towards the large crystals pertains only due to the solubility difference (10%) assumed to exist between the crystals and clusters, thus the

conventional Viedma ripening process is carried out at near-equilibrium conditions ($S_i \approx 1.01$ in Figure 3 bottom right).

In the case of the coupled crystal transformation and Viedma ripening, in Figure 3 (top left), the system initially contains metastable racemic crystals (80%) and seed crystals of the D enantiomer (20%), again giving $\varepsilon_s(0)=20\%$ in favor of the D enantiomer. In Figure 3 (top left) initially, the mass of the racemic crystals and conglomerate D seed crystals is decreasing due to dissolution, leading to an increase in the solution concentration for both enantiomers (Figure 3, bottom left). As the D enantiomer is initially depleted from both the racemic crystals and the seeds, it reaches saturation first. Due to the higher solubility of the racemic compound, a steady mass flux from the racemic crystals to the liquid phase is maintained for both enantiomers, eventually leading to a supersaturated liquid phase with respect to both enantiomers. Supersaturation of the D enantiomer is consumed by growth of the D seeds and D clusters formed by grinding, but since no seeds of the L enantiomer are present, supersaturation builds-up for this enantiomer (Figure 3 bottom left). In this simulation, even though S_L reaches a relatively high value ($S_{L,max} = 1.18$) only a very small amount of mass in L clusters nucleates. The nucleation of the L enantiomer is greatly suppressed here, as a consequence of the concurrent fast racemization, converting part of the excess L molecules to their antipode, which depletes the supersaturation before it results in the nucleation of counter enantiomer mass. Eventually, once the racemic compound is fully dissolved and the supersaturation depletes, the remaining mass in the clusters of the L enantiomer in the solid phase slowly undergo preferential re-dissolution, driving the system to a single chirality.

We suggest that, since nucleation of the counter enantiomer is prevented to a large extent, deracemization essentially proceeds via similar mechanisms as a SOAT process ²², leading to different kinetics compared to Viedma ripening: in the crystal transformation-enhanced deracemization process there is no need for the whole counter enantiomer conglomerate mass to (gradually) pass from the solution phase through breakage and dissolution and convert to the preferred enantiomer, which leads to a faster process. Generally, in SOAT processes, supersaturation is often generated by cooling ²⁷ or evaporation ^{57,58}, while in this process the rate of supersaturation generation depends on the dissolution of the racemic compound, which increases the concentration of both enantiomers in the liquid phase. In a typical SOAT process, ε_s remains constant at 100%, and the preferred enantiomer mass increases due to preferential crystallization. However, in crystal transformation-enhanced deracemization ε_s increases during the process as the racemic compound crystals dissolve and the preferred enantiomer crystallizes.

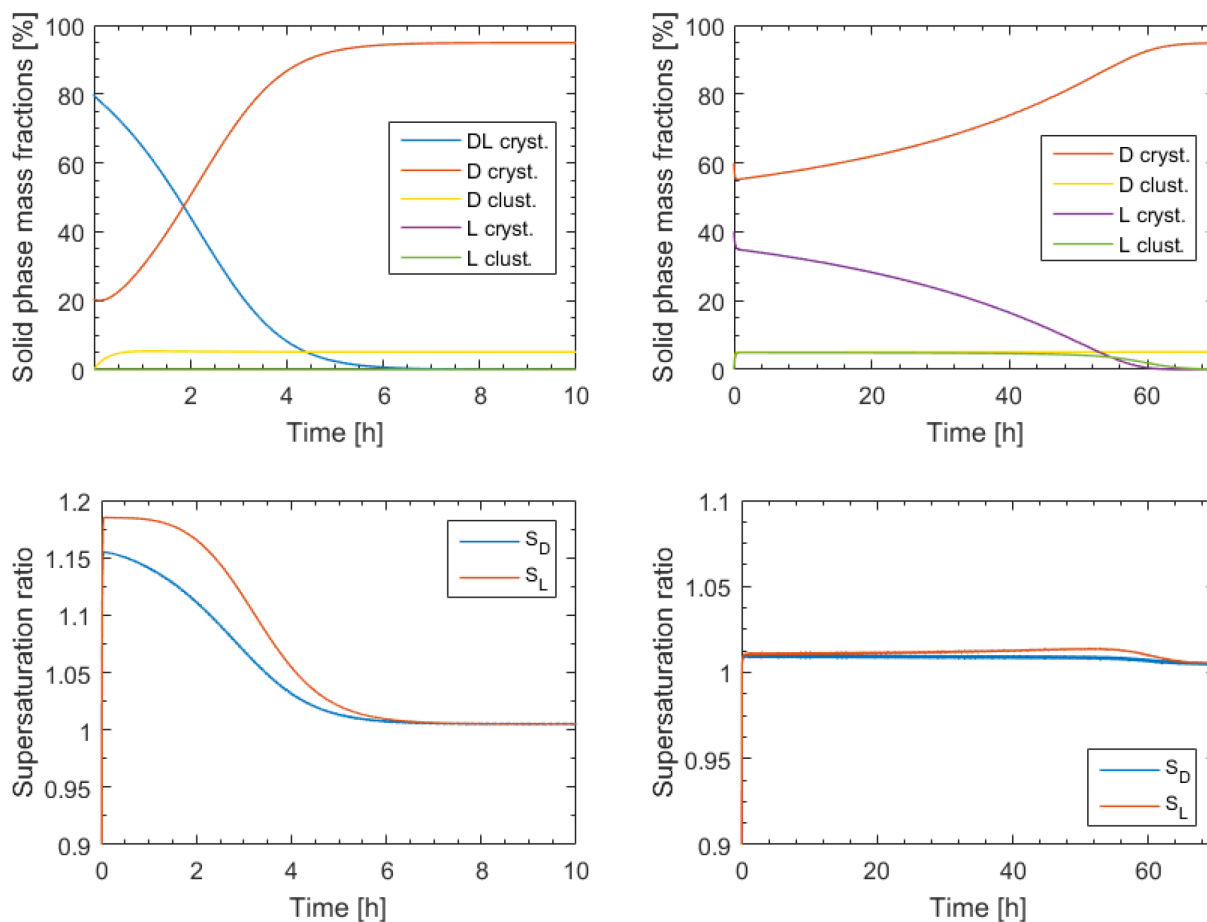


Figure 3. Upper Row: Time evolution of solid phase composition during deracemization including crystal transformation (left) and conventional Viedma ripening without transformation (right). Bottom row: Evolution of supersaturation ratio S_i for the two enantiomers during deracemization including crystal transformation (left) and conventional Viedma ripening without transformation (right).

3.2 Crystal transformation without agglomeration and/or breakage

In computational models of conventional Viedma ripening, the absence of grinding and/or cluster agglomeration does not lead to any increase in the enantiomeric excess^{46,59}. However, we find that solid state deracemization can also be attained if a crystal transformation rather than

grinding and cluster agglomeration is included (Figure 4). The latter processes may not be needed to explain the observed increase in the enantiomeric excess if a crystal transformation is included. In Figure 4, we present simulation results for two different values of the racemization rate constant: $\rho = 10 \text{ h}^{-1}$ and $\rho = 100 \text{ h}^{-1}$, using the same parameters and initial conditions as in the previous section ($\alpha' = \alpha = 2 \text{ mL mg}^{-1} \text{ h}^{-1}$, $\beta = 1 \text{ h}^{-1}$, $\gamma = 0.2 \text{ mL mg}^{-1} \text{ h}^{-1}$, $\nu = \nu' = 0.01 \text{ mL mg}^{-1} \text{ h}^{-1}$), but setting either breakage ($\beta=0$) or agglomeration ($\gamma = \nu' = 0$) or both processes ($\beta = \gamma = \nu' = 0$) to zero.

In Figure 4 (top left), the evolution of ε_s is presented, varying ρ , including breakage and agglomeration. In both cases, a relatively fast increase in ε_s up to 100% is observed. However, for the simulation with $\rho = 10 \text{ h}^{-1}$, the rate of enantiomeric enrichment slows down significantly after reaching a (high in this case) critical value of the enantiomeric excess ($\varepsilon_s \approx 90\%$). Further analysis of these simulations shows that nucleation of the counter enantiomer eventually occurs around the time of attainment of the critical ε_s value, leading to slower deracemization kinetics. At a lower racemization rate, the excess of the counter enantiomer molecules in the liquid phase are not converted to their antipode fast enough, thereby leading to higher supersaturation for the counter enantiomer and higher probability for nucleation. Nonetheless, homochirality is finally achieved through Viedma ripening.

In the absence of breakage ($\beta=0$) but in the presence of agglomeration ($\gamma = 0.2 \text{ mL mg}^{-1} \text{ h}^{-1}$ and $\nu' = 0.01 \text{ mL mg}^{-1} \text{ h}^{-1}$), Figure 4 (bottom left), ε_s increases again up to 100% for the simulation with $\rho = 100 \text{ h}^{-1}$. However, when $\rho = 10 \text{ h}^{-1}$, a plateau value in ε_s is attained. In the absence of breakage and for low racemization rate, seed crystals remain large, but clusters are still formed in the nucleation process for both enantiomers. The mass of clusters formed is higher

for the minor enantiomer as it is not consumed by agglomeration to larger crystals. Eventually, crystals of the minor enantiomer form due to cluster self-agglomeration. Once the cluster mass for each enantiomer depletes either by dissolution or agglomeration, the system attains equilibrium containing only large crystals of both enantiomers and ε_s no longer increases. Note, that complete deracemization is still possible, provided that the nucleation process is suppressed (e.g. for high values of ρ) and is then driven mainly by the dissolution of the racemic crystals and growth of the seeds. However, we note that in real systems, breakage is expected to have a positive influence on the deracemization rate even if no nucleation occurs, due to the increased dissolution rate of the metastable crystals (an effect not accounted for in this model).

In the absence of agglomeration ($\gamma = \nu' = 0$) but in the presence of breakage ($\beta = 1 \text{ h}^{-1}$), Figure 4 (bottom right), for $\rho = 100 \text{ h}^{-1}$, an increase in ε_s is again attained up to 100%. However, the increase is less pronounced than the case with agglomeration (Figure 4, top left). The reason is that in the absence of agglomeration, a higher fraction of the preferred enantiomer mass is present in clusters compared to the case with agglomeration. This in turn leads to a slightly higher concentration of the preferred enantiomer in the solution phase, which slightly decreases the driving force for the dissolution of the racemic compound crystals. Since in the beginning of the process, dissolution of the racemic crystals drives deracemization, the kinetics of deracemization are slower when agglomeration is excluded. For the simulation at $\rho = 100 \text{ h}^{-1}$, a plateau value of ε_s is attained, similarly to the case without breakage. In the presence of intense breakage without agglomeration, all the seed mass of the preferred enantiomer eventually is transferred to clusters (all seeds break down to clusters), while clusters of the counter enantiomer also nucleate. Once the racemic compound dissolves completely and supersaturation depletes for both enantiomers, the system containing only clusters (no size difference between the

enantiomers) of both enantiomers reaches equilibrium and ε_s does not increase further. Again, complete deracemization is possible if the nucleation of the counter enantiomer is suppressed by sufficiently fast racemization and it mainly depends on the dissolution rate of the racemic crystals and growth of the seeds.

Interestingly, in the absence of both breakage and agglomeration ($\beta=\gamma=\nu'=0$), Figure 4 (top right) complete deracemization is achieved regardless of the Q values tested. Additionally, the rate of deracemization is similar to the case where breakage and agglomeration are included (Figure 4, top left). When both breakage and agglomeration are excluded, the seeds of the preferred enantiomer maintain a large size, while the counter enantiomer is formed exclusively as clusters in the nucleation process. Consequently, after the complete dissolution of the racemic crystals and the depletion of the supersaturation, the system will contain a size imbalance between the enantiomers³¹. As a result, the clusters of the counter enantiomer dissolve and the large crystals of the preferred enantiomer grow leading to a single chirality. In real systems, the clusters would of course grow to a larger size, but the conclusions still hold if it is assumed that the clusters cannot outgrow the seed crystals in size and that the overall crystal size remains small ($< 10 \mu\text{m}$). It is noted, that a similar effect is found also for $\beta \neq 0$, but for such low values of β that prevent the complete breakage of the large seeds, allowing for some large crystals of the preferred enantiomer to survive during the deracemization process.

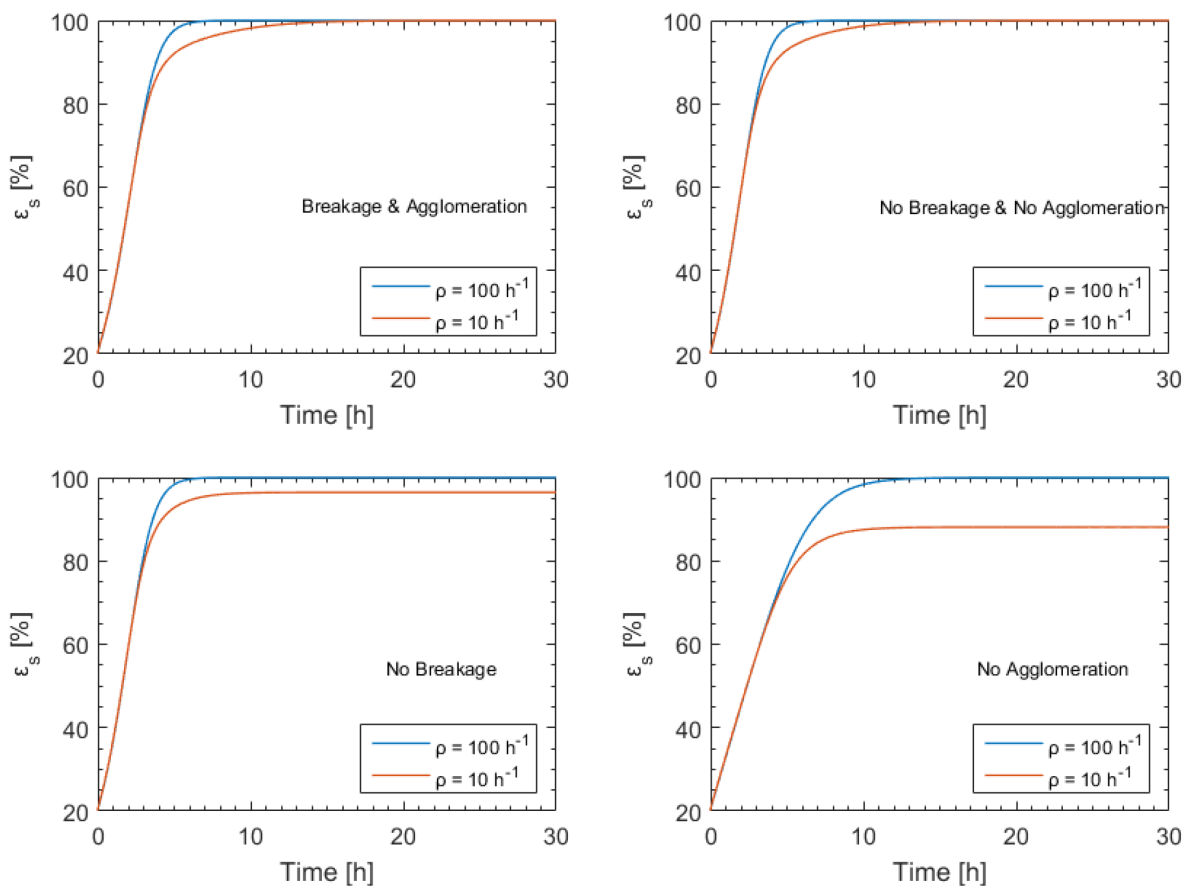


Figure 4. Simulated evolution of the enantiomeric excess ε_s during deracemization including crystal transformation with breakage and agglomeration (top left), without breakage, $\beta=0$, (bottom left), without agglomeration, $\gamma=\nu'=0$ (bottom right) and without both breakage and agglomeration, $\beta=\gamma=\nu'=0$, (top right) with the same remaining parameters.

3.2 Crystal transformation without racemization

In Viedma ripening experiments, usually the racemization catalyst is added after some time of grinding the conglomerate crystals in the solvent. As deracemization does not proceed in the absence of solution phase racemization, this initial time does not influence the process significantly. However, in the combined Viedma ripening-crystal transformation process, the

transformation progresses even without racemization. In order to investigate the influence of the racemization reaction, we carry out a simulation in which the racemization rate is zero ($\rho=0$), keeping the remaining parameters the same ($\alpha' = \alpha = 2 \text{ mL mg}^{-1} \text{ h}^{-1}$, $\beta = 1 \text{ h}^{-1}$, $\gamma = 0.2 \text{ mL mg}^{-1} \text{ h}^{-1}$, $\nu = \nu' = 0.01 \text{ mL mg}^{-1} \text{ h}^{-1}$). The results of this simulation are shown in Figure 5, where the temporal evolution of the composition of all phases is presented.

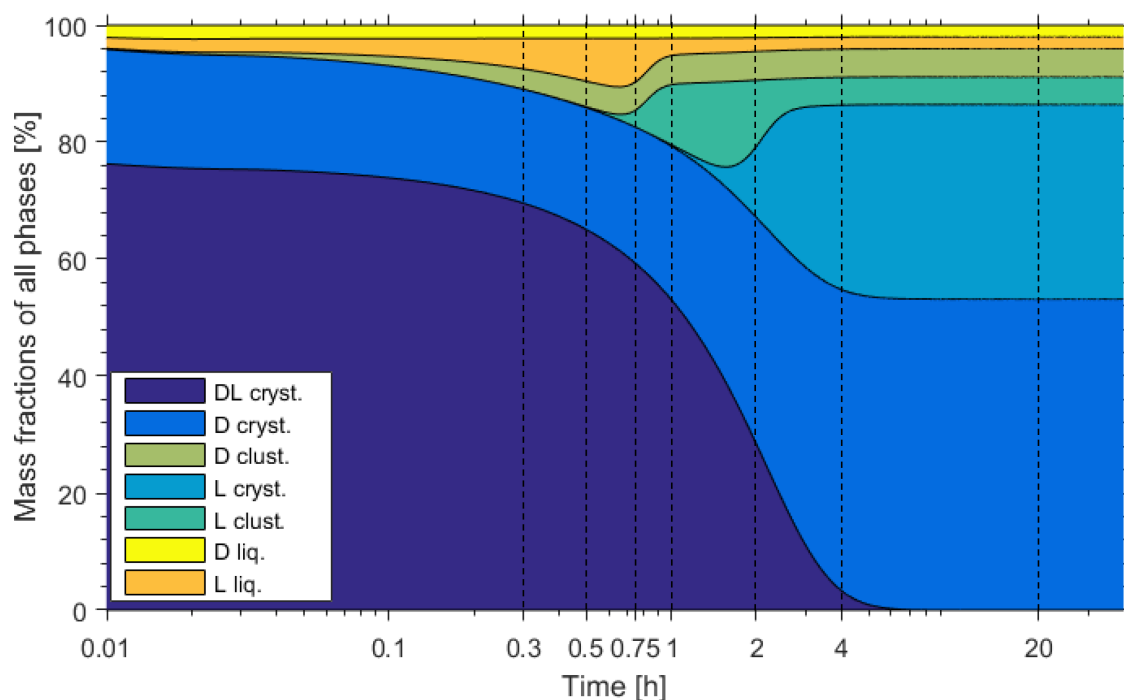


Figure 5. Simulated evolution of the mass fractions of all phases (%) starting from a mixture of metastable racemic crystals (80%) and seed crystals of the *D* enantiomer (20%) in the absence of racemization.

In Figure 5, initially ($0 \text{ h} < t < 0.15 \text{ h}$) mass from both crystal populations (racemic crystals and seeds) partially dissolves, as the solution is undersaturated with respect to both enantiomers, leading to an increase in the solution-phase molecules for both chiralities. Since the preferred enantiomer (*D* in this case) is initially depleted from both the seeds and racemic crystals, it

reaches saturation first ($t \approx 0.01$ h), as there is no racemization reaction to convert the excess molecules. As a result, the seed crystals of the preferred enantiomer start to grow ($t > 0.3$ h) depleting molecules of the same chirality from the solution phase. Since a net transfer of molecules of both chiralities in equal amounts is maintained by the continuous dissolution of the racemic crystals, growth of the *D* seeds is also maintained. As a result, an excess of the molecules of the unwanted enantiomer (*L* in this case) finally prevails (peak excess at $t \approx 0.75$ h), because there are no crystals of that enantiomer present yet to consume these molecules by growth. Eventually, the unwanted enantiomer concentration reaches to a point where nucleation of clusters mass of the same enantiomer starts to occur ($t > 0.75$ h). This mass of clusters reaches a maximum at around $t \approx 2$ h, after which the solution phase is depleted to such extent that nucleation is no longer possible and only net growth occurs. During the following period ($2 \text{ h} < t < 4 \text{ h}$) mass from clusters of the unwanted enantiomer agglomerates to give same chirality crystals. Finally, at $t \approx 20$ h, all of the racemic compound has dissolved and the system contains a racemic liquid phase (4%) and a solid phase of conglomerate crystals of both chiralities (96%). The ε_s is slightly increased from 20% to 20.8% due to the partial dissolution of the initially scalemic mixture. As expected, in the absence of solution-phase racemization, no deracemization occurs.

3.3 Effect of the transformation time prior to deracemization

In the experimental study of Engwerda et al., it was found that varying the racemic crystal transformation time under grinding conditions prior to the addition of the racemization catalyst (often referred to as homogenization time, t_h) had a strong influence on the total deracemization time (Figure 6, right) ³⁰. More specifically, it was found that when t_h was kept short,

deracemization kinetics were faster. In order to find out whether our model can reproduce the experimental observations, we run simulations at the same conditions as previously, where we disable the racemization (by setting $\rho=0$) for the times shown in Figure 6 and reported in Table 2. The mass fractions at these times just before racemization is switched on ($\rho=100 \text{ h}^{-1}$) are also shown in Table 2. These simulations are analogous to experiments in which some transformation/grinding time (t_h) is allowed prior to the addition of the racemization catalyst. The evolution of ε_s for these simulations after t_h is presented in Figure 6.

Table 1. Values of the D and L enantiomer mass fractions for all phases at t_h before racemization is switched on.

Homogenization time (h)	D and L mass fractions in the various phases (%)						
	DL cryst.	D cryst.	D clust.	L cryst.	L clust.	D liq.	L liq.
0.3	69.46	19.50	3.50	0.00	0.01	2.27	5.26
0.5	65.00	20.86	4.38	0.00	0.15	2.26	7.35
0.75	59.18	23.34	4.83	0.00	3.03	2.25	7.37
1	53.07	26.27	4.97	0.24	10.24	2.23	2.98
2	28.31	38.77	4.92	12.25	11.26	2.15	2.34
4	3.33	51.47	4.83	31.53	4.75	2.03	2.06
20	0.00	53.18	4.81	33.26	4.72	2.01	2.02

It appears that deracemization is the fastest when the initial transformation/grinding times are kept short ($t_h= 0.3\text{-}0.75 \text{ h}$). At such short times, no significant mass of clusters of the counter enantiomer have nucleated yet (Table 2), even though supersaturation for nucleation of the

counter enantiomer exists. The initiation of racemization at this point results in the conversion of counter enantiomer molecules to the preferred enantiomer, diminishing the supersaturation for the counter enantiomer thus leading to substantially reduced nucleation for that enantiomer. As a result, only a few counter enantiomer conglomerate crystal mass has to be converted in the deracemization process and the kinetics are faster, directed mainly by the dissolution rate of the remaining racemic crystal phase and the growth rate of the conglomerate seeds. If the conditions are such that nucleation of the counter enantiomer is almost completely prevented ($t_h < 0.3$ h), deracemization essentially proceeds only via SOAT and Viedma ripening does not play a major role in the evolution of ε_s , as shown in previous section. When homogenization times are intermediate ($t_h = 1-2$ h), racemic crystals still exist, but significant mass of counter enantiomer conglomerate phase has also nucleated (Table 2). The deracemization profile for these simulations is fast initially, corresponding to the fast dissolution of the remaining racemic crystals and growth of the preferred enantiomer. However, once the racemic crystal phase is completely dissolved, the remaining counter enantiomer conglomerate phase has to be converted to the preferred chirality via the Viedma ripening mechanisms leading to slower deracemization kinetics. Finally, when the homogenization times are long ($t_h = 20$ h) all the racemic crystals phase has converted to conglomerate (Table 2) before initiation of racemization and thus deracemization is slower as it proceeds only via conventional Viedma ripening. Figure 7, presents the fraction of the counter enantiomer mass that converts to the preferred enantiomer via the Viedma ripening or SOAT mechanisms as a function of the homogenization time. For short values of t_h deracemization proceeds mainly by SOAT, while for longer t_h the contribution of Viedma ripening mechanisms to deracemization become increasingly important. For $t_h = 1$ h, almost half of the counter enantiomer converts directly to the preferred enantiomer via SOAT,

while the other half first nucleates as conglomerate crystals and is later converted to the preferred enantiomer through Viedma ripening. Intriguingly, when no homogenization time is allowed ($t_h=0$), although deracemization proceeds purely by SOAT, the kinetics are slightly slower than when $t_h=0.3$ h (not shown here), similarly to the experimental study. In this case, at the very early stages of the process, when the solution is undersaturated with respect to both enantiomers, the preferred enantiomer builds up a higher concentration in the liquid phase, since it dissolves from both the seeds and the racemic crystals. If the racemization catalyst is present from the beginning, conversion of the preferred enantiomer molecules occurs for a limited amount of time resulting in a decrease in the deracemization kinetics. The results of the model are again in qualitative agreement with the experiments of Engwerda and coworkers³⁰ (Figure 6, right).

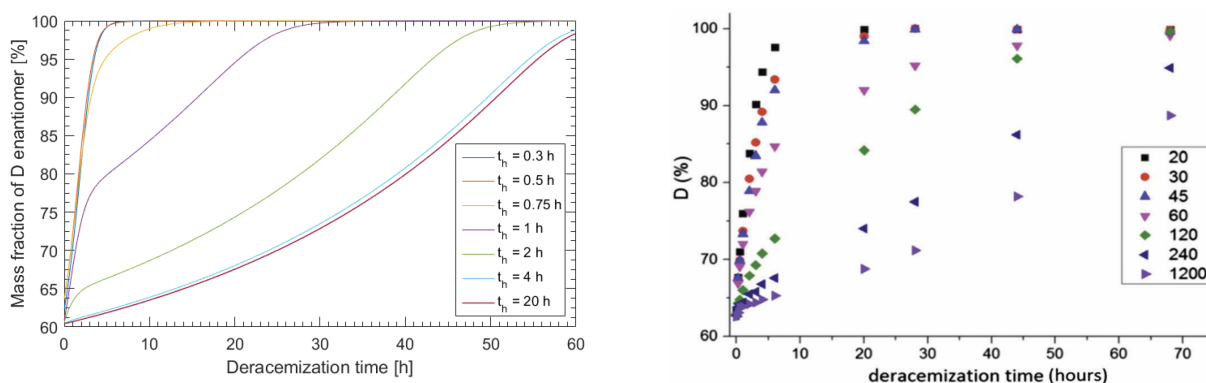


Figure 6. Left: Simulated evolution of the enantiomeric excess ε_s during Viedma ripening coupled with transformation varying the homogenization time t_h at same conditions ($\alpha' = \alpha = 2$ mL mg^{-1} h^{-1} , $\beta = 1$ h^{-1} , $\gamma = 0.2$ mL mg^{-1} h^{-1} , $\nu = \nu' = 0.01$ mL mg^{-1} h^{-1} and $\rho = 100$ h^{-1}). Right: Experimental results of the evolution of the preferred enantiomer (D) solid phase fraction with transformation varying the homogenization time (min), reproduced by permission from Engwerda *et al.*, Chem. Commun., **52**, 12049 (2016). Copyright 2016 Royal Society of Chemistry. In both graphs, the homogenization time is not included in the deracemization time.

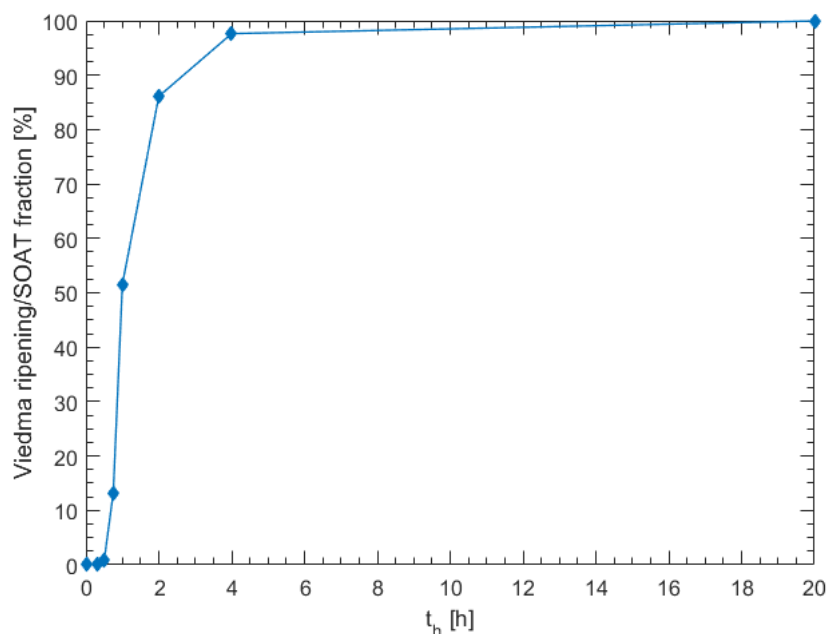


Figure 7. Fraction of the counter enantiomer that converts to the preferred enantiomer via Viedma ripening or SOAT processes as a function of the homogenization time t_h .

3.4 Effect of the (metastable) solubility of the racemic compound

So far in all simulations, we have treated the relative solubility of the racemic compound with respect to the racemic conglomerate (double that of the pure enantiomers) as a constant ($R = C_{eq}^R/2C_{eq}^B = 4.7/4 = 1.175$). However, by carrying out deracemization experiments with transformation at different conditions (*e.g.* temperature), the relative solubilities of the two phases for a given compound will change, influencing the value of R . In the extreme case, where the two phases are enantiotropically related, a transition temperature exists, where $R=1$ and the two phases can co-exist in stable thermodynamic equilibrium. In cases where the racemic compound is a solvate (*e.g.* *DL*-glutamic acid monohydrate³¹), the solubility difference with the racemic conglomerate could be very high in a different solvent, where the solvated compound

would be highly unstable, leading to extreme values for R ⁶⁰. In these cases, dissolution of the racemic compound solvate would also decrease the solvent fraction influencing further the relative solubility during the deracemization process⁶¹. In view of practical applications, it is interesting to have an estimate on the influence of the value of R on the deracemization process when a transformation is included, as this could lead to an optimization strategy for *e.g.* the temperature of the experiment or the feed rate for the racemic compound.

Figure 8, shows simulation results ($\varepsilon_s(0) = 1\%$, $\alpha' = \alpha = 2 \text{ mL mg}^{-1} \text{ h}^{-1}$, $\beta = 1 \text{ h}^{-1}$, $\gamma = 0.2 \text{ mL mg}^{-1} \text{ h}^{-1}$, $\nu = \nu' = 0.01 \text{ mL mg}^{-1} \text{ h}^{-1}$ and $\rho = 100 \text{ h}^{-1}$) varying C_{eq}^R at constant $C_{eq}^B = 2 \text{ mg mL}^{-1}$, which gives values of R between 1.15 and 12. As shown in Figure 8 (top left), increasing R has a strong influence on the dissolution kinetics for the racemic crystals, as the driving force for dissolution, increases significantly (Equation 8). The deracemization profiles for the same simulations are also presented in Figure 8 (top right). For values of C_{eq}^R close to $2C_{eq}^B$ (R values of 1.15 - 1.5), the total deracemization time is relatively short and the kinetic profiles are almost identical to the dissolution kinetics of the racemic crystal phase: deracemization is predominantly controlled by the dissolution of the racemic crystal phase and the subsequent growth of the preferred enantiomer phase. As R increases (3-12) deracemization is faster initially, corresponding to the faster dissolution of the racemic crystals. However, right after the complete dissolution of the racemic crystals, a critical value of ε_s is attained and deracemization slows down, exhibiting similar trend to the one observed during Viedma ripening experiments and simulations. For these simulations, despite the initial rapid ε_s increase, the total deracemization time is longer than those with R values of 1.2-1.5.

The dissolution rate of the racemic crystals influences the rate of supersaturation generation for the counter enantiomer and the nucleation process, as seen in Figure 8 (bottom left). For low values of R (1.15-1.5), supersaturation for the counter enantiomer remains limited, leading to the formation of less clusters for that enantiomer. On the contrary, at higher R values (3-12), supersaturation is rapidly generated, leading to the nucleation of a significant mass of clusters. The time when supersaturation is depleted for each value of R , matches approximately the time when the critical value of ε_s is attained and the deracemization slows. In our simulations, increasing R generally leads to faster initial deracemization. However, the fastest complete deracemization is obtained for $R=1.3$, as shown in Figure 8 (bottom right), which shows that there is an optimal value of C_{eq}^R with respect to $2C_{eq}^B$ above which further increase in C_{eq}^R will cause the opposite effect (decrease in the deracemization time), due to excessive nucleation of the counter enantiomer.

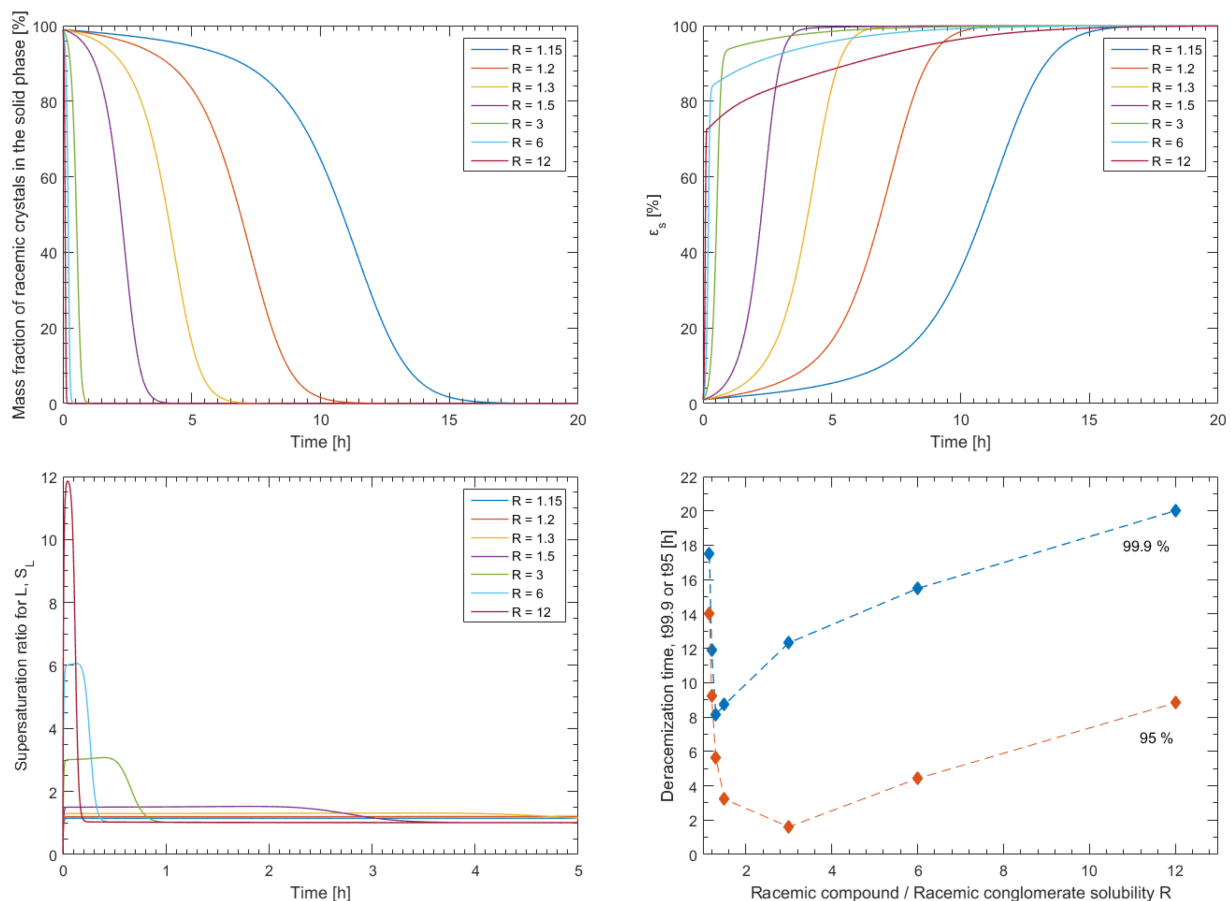


Figure 8. Deracemization simulations at different values of R (1.15-12), dissolution of the racemic crystals (top left), evolution of ϵ_s (top right), evolution of the supersaturation for the counter enantiomer (bottom left) and total time to $\epsilon_s = 95\%$ (orange) or $\epsilon_s = 99.9\%$ (blue) as a function of R (bottom right).

5. CONCLUSIONS

In this study, we extend the cluster model typically used to describe Viedma ripening, to cover the very recently reported cases^{30,31} in which a racemic crystal transformation takes place concurrently with deracemization. Even though here we focus on racemic crystal transformations, the presented model should also be applicable to other types of accelerated

deracemizations involving in-situ gradual feed (*e.g.* reaction-induced conglomerate precipitation or achiral crystal to conglomerate transformation etc.), after minor modifications. The model is able to qualitatively reproduce recent experimental observations and reveals that combining Viedma ripening with a racemic to conglomerate crystal transformation can lead to complete deracemization, but depending on the crystal transformation process there are two ways this could happen: a) nucleation of the counter enantiomer is prevented by the in-situ racemization, thus deracemization is driven mainly by the dissolution of the racemic crystals and growth of the conglomerate seeds (SOAT), or b) nucleation of the counter enantiomer occurs and Viedma ripening is required to convert the counter enantiomer conglomerate crystals. In the former case, mechanisms active in Viedma ripening (breakage, agglomeration), although they may speed-up the process, are not required to explain the observed deracemization. In the latter case, the evolution of the enantiomeric excess is initially controlled by the dissolution rate of the metastable racemic crystals, but once the counter enantiomer nucleates, deracemization proceeds via Viedma ripening leading to slower kinetics. Nucleation of the counter enantiomer may be prevented by controlling the rate of supersaturation generation for the counter enantiomer, directed primarily by the dissolution of the racemic crystals. Best results will be attained for: a) fast racemization kinetics, b) low initial amounts (or gradual feed) of the racemic compound and c) carrying out the deracemization at conditions (*e.g.* temperature, solvent) where the relative solubility between the racemic crystals and racemic conglomerate is not too high. Finally, the combination of Viedma ripening with a racemic crystal transformation can be employed to improve both Viedma ripening and SOAT processes. For Viedma ripening, a higher deracemization rate is attained as the dissolution of the metastable racemic crystals leads

deracemization initially. For SOAT processes, Viedma ripening serves to correct for the accidental nucleation of the counter enantiomer²⁸.

AUTHOR INFORMATION

Corresponding Author

* Email: Georgios.Stefanidis@cit.kuleuven.be

Author Contributions

The manuscript was written through contributions of all authors. All authors have given approval to the final version of the manuscript.

Notes

The authors declare no competing financial interest.

ACKNOWLEDGEMENT

C.X. acknowledges funding of a Ph.D. fellowship by the Research Foundation-Flanders (FWO). J.H.t.H. thanks the EPSRC Centre for Innovative Manufacturing in Continuous Manufacturing and Crystallization (<http://www.cmac.ac.uk>) for supporting this work (EPSRC funding under Grant Reference: EP/I033459/1).

SYMBOLS

C_i^R	mass concentration of <i>D/L</i> enantiomers in racemic crystals [mg mL ⁻¹]
C_i^B	mass concentration of <i>D/L</i> enantiomers in big crystals [mg mL ⁻¹]
C_i^S	mass concentration of <i>D/L</i> enantiomers in small clusters [mg mL ⁻¹]
C_i^{liq}	mass concentration of <i>D/L</i> enantiomers in the solution phase [mg mL ⁻¹]
C_{eq}^B	equilibrium mass concentration of <i>D</i> or <i>L</i> enantiomer in the solution phase in contact

	with crystals [mg mL ⁻¹]
C_{eq}^S	equilibrium mass concentration of <i>D</i> or <i>L</i> enantiomer in the solution phase in contact with clusters [mg mL ⁻¹]
C_{eq}^R	equilibrium mass concentration of both <i>D</i> and <i>L</i> enantiomer in the solution phase in contact with racemic crystals [mg mL ⁻¹]
G_i^R	growth/dissolution rate of the racemic crystals [mg mL ⁻¹ h ⁻¹]
G_i^B	growth/dissolution rate of large crystals [mg mL ⁻¹ h ⁻¹]
G_i^S	growth/dissolution rate of clusters [mg mL ⁻¹ h ⁻¹]
J_i	nucleation rate of clusters [mg mL ⁻¹ h ⁻¹]
B_i	breakage rate of large crystals [mg mL ⁻¹ h ⁻¹]
A_i	agglomeration rate of clusters with themselves and with large crystals [mg mL ⁻¹ h ⁻¹]
r_i	racemization rate [mg mL ⁻¹ h ⁻¹]
α'	rate constant for growth/dissolution of the racemic crystals [mL mg ⁻¹ h ⁻¹]
α	rate constant for growth/dissolution of crystals and clusters [mL mg ⁻¹ h ⁻¹]
ν	rate constant for the nucleation of clusters [mL mg ⁻¹ h ⁻¹]
β	rate constant for breakage of large crystals [h ⁻¹]
ν'	rate constant for the cluster self-agglomeration [mL mg ⁻¹ h ⁻¹]
γ	rate constant for the agglomeration of clusters to crystals [mL mg ⁻¹ h ⁻¹]
ρ	rate constant for the solution-phase racemization reaction [h ⁻¹]
t	Time [h]
t_h	homogenization time, <i>i.e.</i> grinding/transformation time prior to the addition of the racemization catalyst [h]
S_i	supersaturation ratio for <i>D/L</i> enantiomers (with respect to large crystals)
ε_l	liquid phase enantiomeric excess [%]
ε_s	solid phase enantiomeric excess [%]
R	relative solubility of the racemic compound with respect to racemic conglomerate

REFERENCES

- (1) Viedma, C. *Phys. Rev. Lett.* **2005**, *94*, 3–6.
- (2) Noorduyn, W. L.; Vlieg, E.; Kellogg, R. M.; Kaptein, B. *Angew. Chemie - Int. Ed.* **2009**, *48*, 9600–9606.
- (3) Sögütoglu, L. C.; Steendam, R. R. E.; Meekes, H.; Vlieg, E.; Rutjes, F. P. J. T. *Chem. Soc. Rev.* **2015**, *44*, 6723–6732.
- (4) Noorduyn, W. L.; Izumi, T.; Millemaggi, A.; Leeman, M.; Meekes, H.; Van Enkevort, W. J. P.; Kellogg, R. M.; Kaptein, B.; Vlieg, E.; Blackmond, D. G. *J. Am. Chem. Soc.* **2008**, *130*, 1158–1159.
- (5) Viedma, C.; Ortiz, J. E.; De Torres, T.; Izumi, T.; Blackmond, D. G. *J. Am. Chem. Soc.* **2008**, *130*, 15274–15275.
- (6) Spix, L.; Meekes, H.; Blaauw, R. H.; Van Enkevort, W. J. P.; Vlieg, E. *Cryst. Growth Des.* **2012**, *12*, 5796–5799.
- (7) Wilmlink, P.; Rougeot, C.; Wurst, K.; Sanselme, M.; Van Der Meijden, M.; Saletta, W.; Coquerel, G.; Kellogg, R. M. *Org. Process Res. Dev.* **2015**, *19*, 302–308.
- (8) Kellogg, R.; Van der Meijden, M.; Leeman, M.; Gelens, E.; Noorduyn, W.; Meekes, H.; Van Enkevort, W.; Kaptein, B.; Vlieg, E. *Org. Process Res. Dev.* **2009**, *13*, 1195–1198.
- (9) Noorduyn, W. L.; Kaptein, B.; Meekes, H.; Van Enkevort, W. J. P.; Kellogg, R. M.; Vlieg, E. *Angew. Chemie - Int. Ed.* **2009**, *48*, 4581–4583.
- (10) Steendam, R. R. E.; Brouwer, M. C. T.; Huijs, E. M. E.; Kulka, M. W.; Meekes, H.; Van Enkevort, W. J. P.; Raap, J.; Rutjes, F. P. J. T.; Vlieg, E. *Chem. - A Eur. J.* **2014**, *20*, 13527–13530.
- (11) Iggländ, M.; Mu, R.; Mazzotti, M.; Müller, R.; Mazzotti, M. *Cryst. Growth Des.* **2014**, *14*, 2488–2493.
- (12) Iggländ, M.; Mazzotti, M. *CrystEngComm* **2013**, *15*, 2319.
- (13) Kaptein, B.; Noorduyn, W. L.; Meekes, H.; Van Enkevort, W. J. P.; Kellogg, R. M.; Vlieg, E. *Angew. Chemie - Int. Ed.* **2008**, *47*, 7226–7229.
- (14) Hein, J. E.; Huynh Cao, B.; Viedma, C.; Kellogg, R. M.; Blackmond, D. G. *J. Am. Chem. Soc.* **2012**, *134*, 12629–12636.
- (15) Xiouras, C.; Van Aeken, J.; Panis, J.; Ter Horst, J. H.; Van Gerven, T.; Stefanidis, G. D. *Cryst. Growth Des.* **2015**, *15*, 5476–5484.
- (16) Steendam, R. R. E.; Harmsen, B.; Meekes, H.; Van Enkevort, W. J. P.; Kaptein, B.; Kellogg, R. M.; Raap, J.; Rutjes, F. P. J. T.; Vlieg, E. *Cryst. Growth Des.* **2013**, *13*, 4776–4780.

- (17) Noorduin, W. L.; Van Der Asdonk, P.; Meekes, H.; Van Enkevort, W. J. P.; Kaptein, B.; Leeman, M.; Kellogg, R. M.; Vlieg, E. *Angew. Chemie - Int. Ed.* **2009**, *48*, 3278–3280.
- (18) Steendam, R. R. E.; Dickhout, J.; Van Enkevort, W. J. P.; Meekes, H.; Raap, J.; Rutjes, F. P. J. T.; Vlieg, E. *Cryst. Growth Des.* **2015**, *15*, 1975–1982.
- (19) Tarasevych, A. V.; Sorochinsky, A. E.; Kukhar, V. P.; Toupet, L.; Crassous, J.; Guillemin, J.-C. *CrystEngComm* **2015**, *17*, 1513–1517.
- (20) Noorduin, W. L.; Bode, A. A. C.; Van der Meijden, M.; Meekes, H.; Van Etteger, A. F.; Van Enkevort, W. J. P.; Christianen, P. C. M.; Kaptein, B.; Kellogg, R. M.; Rasing, T.; Vlieg, E. *Nat. Chem.* **2009**, *1*, 729–732.
- (21) Havinga, E. *Biochim. Biophys. Acta* **1954**, *13*, 171–174.
- (22) Jacques, J.; Collet, A.; Wilen, S. H. *Enantiomers, racemates, and resolutions*; Wiley, 1981.
- (23) Kondepudi, D. K. K.; Kaufman, R. J. J.; Singh, N. *Science* **1990**, *250*, 975–976.
- (24) Lorenz, H.; Seidel-Morgenstern, A. *Angew. Chemie - Int. Ed.* **2014**, *53*, 1218–1250.
- (25) Levilain, G.; Coquerel, G. *CrystEngComm* **2010**, *12*, 1983.
- (26) Levilain, G.; Rougeot, C.; Guillen, F.; Plaquevent, J. C.; Coquerel, G. *Tetrahedron Asymmetry* **2009**, *20*, 2769–2771.
- (27) Leeman, M.; Noorduin, W. L.; Millemaggi, A.; Vlieg, E.; Meekes, H.; Van Enkevort, W. J. P.; Kaptein, B.; Kellogg, R. M. *CrystEngComm* **2010**, *12*, 2051–2053.
- (28) Steendam, R. R. E.; Van Benthem, T. J. B.; Huijs, E. M. E.; Meekes, H.; Van Enkevort, W. J. P.; Raap, J.; Rutjes, F. P. J. T.; Vlieg, E. *Cryst. Growth Des.* **2015**, *15*, 3917–3921.
- (29) Rougeot, C.; Hein, J. E. *Org. Process Res. Dev.* **2015**, *19*, 1809–1819.
- (30) Engwerda, A. H. J.; Meekes, H.; Kaptein, B.; Rutjes, F. P. J. T.; Vlieg, E. *Chem. Commun.* **2016**, *96*, 1659–1676.
- (31) Xiouras, C.; Van Cleemput, E.; Kumpen, A.; Ter Horst, J. H.; Van Gerven, T.; Stefanidis, G. D. *Cryst. Growth Des.* **2016**, *17*, 882–890.
- (32) Nyvlt, J. *Cryst. Res. Technol.* **1997**, *32*, 695–699.
- (33) Cardew, P. T.; Davey, R. J. *Proc. R. Soc. London. A. Math. Phys. Sci.* **1985**, *398*, 415 LP-428.
- (34) Davey, R. J.; Cardew, P. T.; McEwan, D.; Sadler, D. E. *J. Cryst. Growth* **1986**, *79*, 648–653.

- (35) Noorduin, W. L.; Meekes, H.; Bode, A. A. C.; Van Enkevort, W. J. P.; Kaptein, B.; Kellogg, R. M.; Vlieg, E. *Cryst. Growth Des.* **2008**, *8*, 1675–1681.
- (36) Uwaha, M. *J. Phys. Soc. Japan* **2004**, *73*, 2601–2603.
- (37) Uwaha, M. *J. Phys. Soc. Japan* **2008**, *77*, 6–9.
- (38) Uwaha, M.; Katsuno, H. *J. Phys. Soc. Japan* **2009**, *78*, 2–5.
- (39) Noorduin, W. L.; Van Enkevort, W. J. P.; Meekes, H.; Kaptein, B.; Kellogg, R. M.; Tully, J. C.; McBride, J. M.; Vlieg, E. *Angew. Chemie - Int. Ed.* **2010**, *49*, 8435–8438.
- (40) Wattis, J. A. D. *Orig. Life Evol. Biosph.* **2011**, *41*, 133–173.
- (41) Cartwright, J. H. E.; Piro, O.; Tuval, I. *Phys. Rev. Lett.* **2007**, *98*, 1–4.
- (42) Katsuno, H.; Uwaha, M. *J. Cryst. Growth* **2009**, *311*, 4265–4269.
- (43) Saito, Y.; Hyuga, H. *J. Cryst. Growth* **2011**, *318*, 93–98.
- (44) Ricci, F.; Stillinger, F. H.; Debenedetti, P. G. *J. Chem. Phys.* **2013**, *139*, 174503.
- (45) Skrdla, P. J. *Cryst. Growth Des.* **2011**, *11*, 1957–1965.
- (46) Iggländ, M.; Mazzotti, M. *Cryst. Growth Des.* **2011**, *11*, 4611–4622.
- (47) Gherase, D.; Conroy, D.; Matar, O. K.; Blackmond, D. G. *Cryst. Growth Des.* **2014**, *14*, 928–937.
- (48) Blanco, C.; Ribo, J. M.; Hochberg. *Phys. Rev. E - Stat. Nonlinear, Soft Matter Phys.* **2015**, *91*, 1–13.
- (49) Köllges, T.; Vetter, T. *Cryst. Growth Des.* **2016**, *17*, 233–247.
- (50) Katsuno, H.; Uwaha, M. *Phys. Rev. E - Stat. Nonlinear, Soft Matter Phys.* **2016**, *93*, 1–10.
- (51) Spix, L.; Engwerda, A. H. J.; Meekes, H.; Van Enkevort, W. J. P.; Vlieg, E. *Cryst. Growth Des.* **2016**, *16*, 4752–4758.
- (52) Spix, L.; Van der Wal, L. J. M.; Van Enkevort, W.; Meekes, H.; Vlieg, E. *CrystEngComm* **2016**, *18*, 9252–9259.
- (53) Meyerhoffer, W. *Berichte der Dtsch. Chem. Gesellschaft* **1904**, *37*, 2604–2610.
- (54) Nývlt, J. *J. Cryst. Growth* **1968**, *3*, 377–383.
- (55) Katsuno, H.; Uwaha, M. *J. Cryst. Growth* **2014**, *401*, 59–62.
- (56) Jakubiak, P.; Schuler, F.; Alvarez-Sánchez, R. *Eur. J. Pharm. Biopharm.* **2016**, *109*, 43–

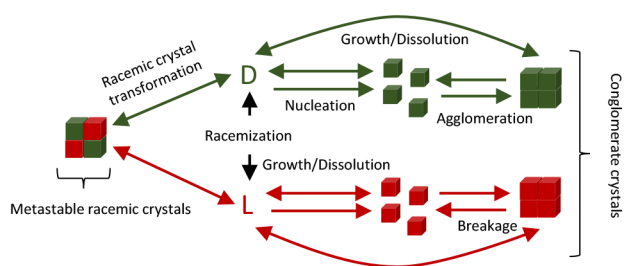
48.

- (57) Black, S. N.; Williams, L. J.; Davey, R. J.; Moffatt, F.; Jones, R. V. H.; McEwan, D. M.; Sadler, D. E. *Tetrahedron* **1989**, *45*, 2677–2682.
- (58) Yagishita, F.; Ishikawa, H.; Onuki, T.; Hachiya, S.; Mino, T.; Sakamoto, M. *Angew. Chemie - Int. Ed.* **2012**, *51*, 13023–13025.
- (59) Noorduin, W. L.; Meekes, H.; Van Enkevort, W. J. P.; Millemaggi, A.; Leeman, M.; Kaptein, B.; Kellogg, R. M.; Vlieg, E. *Angew. Chemie - Int. Ed.* **2008**, *47*, 6445–6447.
- (60) Nordhoff, S.; Ulrich, J. J. *Therm. Anal. Calorim.* **1999**, *57*, 181–192.
- (61) Qu, H.; Louhi-Kultanen, M.; Rantanen, J.; Kallas, J. *Cryst. Growth Des.* **2006**, *6*, 2053–2060.

For Table of Contents Use Only

Coupling Viedma Ripening with Racemic Crystal Transformations: Mechanism of Deracemization

Christos Xiouras, Joop H. Ter Horst, Tom Van Gerven and Georgios D. Stefanidis



In this work, we develop a kinetic model to study the mechanisms through which deracemization occurs when a seeded solvent-mediated racemic crystal transformation to conglomerate takes place under grinding-racemization conditions. The model explains recent experimental observations and shows that the new process leads to fast and complete deracemization through a combination of second order asymmetric transformation (SOAT) and Viedma ripening.